Stator Flux Control by Active Disturbance Rejection Control for DFIG Wind Turbine During Voltage Dip

R. Chakib, M. Cherkaoui, A. Essadki

***Abstract*—** In this paper, we propose a control strategy based on the control loops of ADRC (Active Disturbance Rejection Control) to allow a wind system based on a DFIG (Doubly Fed Induction Generator) to stay connected to the grid during voltage dip, and to resume production of electrical energy within milliseconds after the fault has disappeared. This strategy is essentially based on the control of the stator flux for maintaining the magnetization of the generator during voltage dip, and the use of a crowbar resistive circuit to protect the electronic power converters by limiting rotor currents and the DC bus voltage. The dynamic model of this wind system and the ADRC controllers are simulated in Matlab-Simulink environment.

***Keywords*—**ADRC, Control of stator flux, Crowbar, DFIG, Maximum Power Point Tracking, Voltage dip.

I. Introduction

The development of renewable energy is the best way to deal with the dangers posed globally by the massive use of fossil fuels. It will also satisfy electricity needs of the planet that would increase by 50% or more by 2030 [1]. Renewable electricity comes from six sources: hydroelectric, wind energy, biomass, solar, geothermal and marine energy. Among these renewable energy sources, wind power is the one that has the most important energy potential. The power of the wind turbine installed worldwide is increasing more and more every year. Several studies have been conducted to investigate the integration and the impact of wind power on the distribution grids. Previously, the installed wind power was low, and wind farms had only one constraint: produce electrical energy when there is enough wind and disconnect from the grid in event of default in it. The protection plans consisted, in default, of disconnecting the turbine of the grid and stop it. This implied for the network operator to cope with lack of production for several minutes, the time to reboot and reconnect the turbine to the grid [2]-[13]. Today, due to the significant increase in the installed power of wind farms, the latter are subject to standards and technical requirements imposed by the network operator. By these standards, the wind turbines are required to ensure the continuity of production of electrical energy or at least be capable of resuming production as soon as the fault disappears. In addition to this constraint, the standards in some European countries indicate that wind farms must contribute to the return of voltage by injecting reactive power on the network during a voltage dip [2]. The intermittent nature of wind power production and the increase of its penetration rate in power systems generate several problems for operators such as voltage variation, frequency variation and grid instability. The network operators impose some attachment requirements one the distribution grid of power plants. When a fault occurs and when the drop in voltage is not too high, the turbine must stay connected to the grid and continue to function normally. If the voltage drop is important, the wind turbine must provide reactive power to maintain the level of the voltage supply and contribute to its rapid recovery. In case the voltage drop is too high and/or too long, the wind turbine may be disconnected from the grid [2]-[3]-[4]-[13].

In this paper, we study the behavior of the DFIG used in wind system during voltage dips. The objective is to develop control strategies of the DFIG based on an ADRC method to satisfy the constraint of staying connected during the drop of voltage terminal of the wind turbine. The voltage drop across the DFIG causes an increase of the stator current. Due to the magnetic coupling between the stator and the rotor, a high intensity goes also through the rotor coiling and the rotor side power converter, this leads to an increase of the DC voltage bus [2]-[3]-[7]. Without protection, this can lead to the damage of power converters. A protection system by crowbar circuit is used in this paper to limit the peaks of rotor currents at the appearance and disappearance of the fault. A stator flux control strategy based on an ADRC is proposed in this piece of work to improve the controllability of the DFIG and regain normal operation after the voltage dip.

II. Dynamic Model of the Studied System

The wind system studied in this article is at variable speed. The stator of the DFIG is directly connected to the grid and the rotor is connected to the grid through two power electronic converters separated by a linking DC bus. The grid side converter is connected to the latter by means of a three-phase filter for filtering the current harmonics. The presence of

R. Chakib is with department of Electrical Engineering of Mohammedia School of Engineers (EMI), University Mohammed V, Rabat Morocco (e-mail: RachidChakib@research.emi.ac.ma).

M. Cherkaoui is with department of Electrical Engineering of Mohammedia School of Engineers (EMI), University Mohammed V, Rabat Morocco (e-mail: cherkaoui@emi.ac.ma).

A. Essadki is with department of Electrical Engineering of High School of Technical Education (ENSET), University Mohammed V, Rabat Morocco (e-mail: ahmed.essadki@gmail.com).

converters between the rotor and the grid allows to control the transfer of active and reactive power between the stator and the network (fig.1). These converters are designed to only pass the slip power, (i.e, from 20% to 30% of the rated power of the generator) [7]. In this study, we consider that the blade pitch angle is constant and wind speed never exceeds the rated speed [4]-[5].

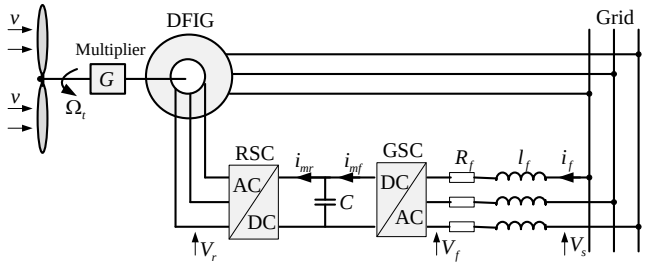

Fig. 1 Diagram of a wind turbine based on a DFIG

A. Wind turbine

The wind turbine extracts a part of the kinetic energy of the wind and drives the DFIG at variable speed through a speed multiplier [6]-[7].

According to Betz law, the aerodynamic performance of the turbine is less than 59.3%. Its aerodynamic power is expressed as a function of its power coefficient as follow:

$$P_{aero} = \frac{1}{2} C_p(\lambda, \beta) \rho \pi R^2 v^3 \quad (1)$$

The power coefficient C_p depends on the blade pitch angle β and the speed ratio λ.

$$C_p(\beta, \lambda) = \frac{1}{2}(116\lambda_i - 0{,}4\beta - 5)e^{(-21\lambda_i)} + 0.0068\lambda \quad (2)$$

where $\lambda_i = \frac{1}{\lambda + 0.08\beta} - \frac{0.035}{1+\beta^3}$ and $\lambda = \frac{\Omega_t R}{v}$

The aerodynamic torque:

$$T_{aero} = \frac{1}{2} C_p(\beta, \lambda) \rho \pi R^2 \frac{v^3}{\Omega_t} \quad (3)$$

R is the radius of the turbine, ρ is the air density, Ω_t is the turbine speed, β is the pitch angle and v is the wind speed.

The multiplier is modeled by a simple gain; its adjusts the speed of the turbine to the generator as follows:

$$\Omega_{mec} = G\Omega_t \quad (4)$$

The evolution of the mechanical speed from the mechanical torque applied to the rotor is given by the following equation:

$$J \frac{d\Omega_{mec}}{dt} = T_{mec} - T_{em} - f\Omega_{mec} \quad (5)$$

where T_{mec} is the mechanical torque, T_{em} is the electromagnetic torque, f is friction coefficient.

B. DFIG

In Park's reference synchronized with the stator flux, the mathematical model of DFIG is given by the following equations [4]-[6]:

$$V_{sd} = R_s i_{sd} + \frac{d\Phi_{sd}}{dt} - \omega_s \Phi_{sq} \quad (6)$$

$$V_{sq} = R_s i_{sq} + \frac{d\Phi_{sq}}{dt} + \omega_s \Phi_{sd} \quad (7)$$

$$V_{rd} = R_r i_{rd} + \frac{d\Phi_{rd}}{dt} - \omega_r \Phi_{rq} \quad (8)$$

$$V_{rq} = R_r i_{rq} + \frac{d\Phi_{rq}}{dt} + \omega_r \Phi_{rd} \quad (9)$$

$$\omega_r = \omega_s - p\Omega_{mec} \quad (10)$$

$$\Phi_{sd} = L_s i_{sd} + L_m i_{rd} \quad (11)$$

$$\Phi_{sq} = L_s i_{sq} + L_m i_{rq} \quad (12)$$

$$\Phi_{rd} = L_r i_{rd} + L_m i_{sd} \quad (13)$$

$$\Phi_{rq} = L_r i_{rq} + L_m i_{sq} \quad (14)$$

$$T_{em} = \frac{3}{2} p \frac{L_m}{L_s} (i_{rd}\Phi_{sq} - i_{rq}\Phi_{sd}) \quad (15)$$

$$P_s = V_{sd} i_{sd} + V_{sq} i_{sq} \quad (16)$$

$$Q_s = V_{sq} i_{sd} - V_{sd} i_{sq} \quad (17)$$

L_s is the cyclic stator inductance, L_r is the cyclic rotor inductance, L_m is the mutual inductance, R_s is stator resistance, R_r is rotor resistance, p is number of pole pairs.

C. Converters

The rotor side converter controls the torque and speed of the turbine. It also allows mastering the magnetic state of the generator and controlling reactive power exchanged between the stator and the grid [4]-[10].

The grid side converter's role is to regulate the Dc bus voltage. This regulation ensures the exchange of active power between the rotor and the grid. This converter is also used for supplying or absorbing reactive power of the grid. Control of the two converters is achieved by pulse width modulation (PWM) [10]-[11].

III. Controllers

To ensure the normal operation of the wind system, three commands are required:

- Command for extracting the maximum power for the wind by a control MPPT.
- Command of the rotor side converter controlling the electromagnetic torque and the stator reactive power of the DFIG.
- Command of the grid side converter controlling the DC bus voltage and active and reactive power exchanged with the grid.

These commands are provided by control loops of the ADRC type. The foundation of the ADRC is based on the use of an ESO (Extended State Observer) which estimates in real time and at the same time the external disturbances and the errors due to variation of system parameters and modeling uncertainties [8]. Figure 2 shows the basic structure of a control loop by ADRC [8]-[14].

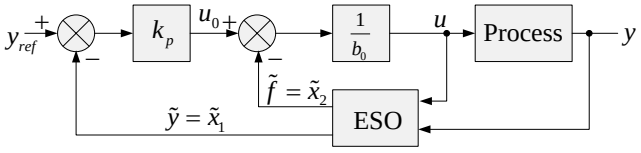

Fig. 2 ADRC topology

A. Control of rotor side converter

By choosing Park's referential linked to the rotating stator field and by directing the stator flux according to d-axis, we simplify the equations of the mathematical model of DFIG assuming R_s is negligible and stator flux Φ_s is constant [3]-[11]-[12].

$$V_{sd} = 0 \quad (18)$$

$$V_{sq} \simeq \omega_s \Phi_{sd} \simeq \omega_s \Phi_s \quad (19)$$

$$V_{rd} = R_r i_{rd} + \sigma L_r \frac{di_{rd}}{dt} - \omega_r \sigma L_r i_{rq} \quad (20)$$

$$V_{rq} = R_r i_{rq} + \sigma L_r \frac{di_{rq}}{dt} + \omega_r \sigma L_r i_{rd} + \omega_r \frac{L_m}{L_s}\Phi_s \quad (21)$$

$$T_{em} = -\frac{3}{2} p \frac{L_m}{L_s}\Phi_s i_{rq} \quad (22)$$

$$P_s = -V_{sq}\frac{L_m}{L_s} i_{rq} \quad (23)$$

$$Q_s = \frac{V_{sq}\Phi_s}{L_s} - \frac{V_{sq}L_m}{L_s} i_{rd} \quad (24)$$

where $= 1 - \frac{L_m^2}{L_s L_r}$: dispersion coefficient between the coilings d and q.

The equations of rotor voltage (20) and (21) can be written as follows:

$$\frac{di_{rd}}{dt} = -\frac{R_r}{\sigma L_r} i_{rd} + \omega_r i_{rq} + \frac{1}{\sigma L_r} V_{rd} \quad (25)$$

$$\frac{di_{rq}}{dt} = -\frac{R_r}{\sigma L_r} i_{rq} - \omega_r i_{rd} - \omega_r \frac{L_m}{\sigma L_r L_s}\Phi_s + \frac{1}{\sigma L_r} V_{rq} \quad (26)$$

The control of this converter is structured around two ADRC control loops of rotor currents i_{rd} and i_{rq}. The expressions (25) and (26) can be put in the canonical form of an ADRC regulator [14]:

$$\frac{di_{rd}}{dt} = f_d + b_0 u_d(t) \quad (27)$$

$$\text{where: } \begin{cases} f_d = -\frac{R_r}{\sigma L_r} i_{rd} + \omega_r i_{rq} + \left(\frac{1}{\sigma L_r} - b_0\right) V_{rd} \\ b_0 = \frac{1}{\sigma L_r} \; ; \; u_d = V_{rd} \end{cases}$$

$$\frac{di_{rq}}{dt} = f_q + b_0 u_q(t) \quad (28)$$

where

$$\begin{cases} f_q = -\frac{R_r}{\sigma L_r} i_{rq} - \omega_r i_{rd} - \omega_r \frac{L_m}{\sigma L_r L_s}\Phi_s + \left(\frac{1}{\sigma L_r} - b_0\right) V_{rq} \\ b_0 = \frac{1}{\sigma L_r} \; ; \; u_q = V_{rq} \end{cases}$$

f_d et f_q are external and internal disturbances respectively affecting the rotor currents i_{rd} and i_{rq}. u_d and u_q are respectively the control inputs of the currents loops i_{rd} and i_{rq}. b_0 is the known part of the system parameters. Figure 3 shows the control loop of rotor currents.

Equations (22) and (23) show that the electromagnetic torque produced by DFIG and active stator power are proportional to the rotor current of q-axis. The reference current i_{rq_ref} is from MPPT control via the electromagnetic torque reference [12].

$$T_{em\_ref} = \frac{1}{2}\frac{C_{pmax}\rho\pi R^5 \Omega_{mec}^2}{\lambda_{opt}^3 G^3} \quad (29)$$

$$i_{rq\_ref} = -\frac{2}{3}\frac{L_s}{pL_m\Phi_s} T_{em\_ref} \quad (30)$$

Equation (24) shows that the reactive stator power is related to current rotor d-axis by a constant imposed by the grid.

$$i_{rd\_ref} = \frac{\Phi_s}{L_m} - \frac{L_s}{V_{sq}L_m} Q_{s\_ref} \quad (31)$$

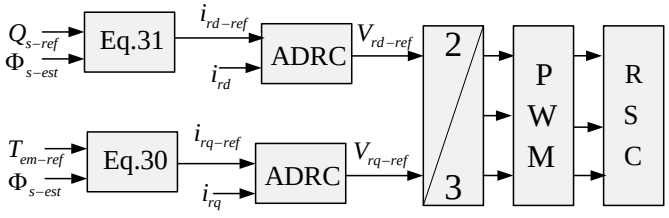

Fig. 3 Control loops of rotor currents

B. Control of grid side converter

Modeling in dq reference of the set of binding to the electric network consisting of the DC bus, the grid side converter and the filter are given by the equation below [6]-[13]:

$$L_f \frac{di_{df}}{dt} + R_f i_{df} + L_f \omega_s i_{qf} = V_{sd} - V_{df} \quad (32)$$

$$L_f \frac{di_{qf}}{dt} + R_f i_{qf} - L_f \omega_s i_{df} = V_{sq} - V_{qf} \quad (33)$$

$$C\frac{dU_{dc}}{dt} = i_{mf} - i_{mr} \quad (34)$$

$$P_f = \frac{3}{2} V_{sq} i_{qf} \quad (35)$$

$$Q_f = \frac{3}{2} V_{sq} i_{df} \quad (36)$$

$$P_{dc} = U_{dc} i_{mf} = P_f \quad (37)$$

The control of this converter can control the currents flowing through the filter and the DC bus voltage (figure 4). To implement the ADRC regulators, we write equations (32) and (33) as follows:

$$\frac{di_{df}}{dt} = f_{df} + b_0 u_{df}(t) \quad (38)$$

$$\text{where: } \begin{cases} f_{df} = \frac{1}{L_f} V_{sd} - \frac{R_f}{L_f} i_{df} - \omega_s i_{qf} + \left(\frac{1}{L_f} - b_0\right) V_{df} \\ b_0 = -\frac{1}{L_f} \; ; \; u_{df} = V_{df} \end{cases}$$

$$\frac{di_{qf}}{dt} = f_{qf} + b_0 u_{qf}(t) \quad (39)$$

$$\text{where: } \begin{cases} f_{qf} = \frac{1}{L_f} V_{sq} - \frac{R_f}{L_f} i_{qf} - \omega_s i_{df} + \left(\frac{1}{L_f} - b_0\right) V_{qf} \\ b_0 = -\frac{1}{L_f} \; ; \; u_{qf} = V_{qf} \end{cases}$$

The reference current i_{df_ref} is determined to impose a zero grid side reactive power.

$$i_{df\_ref} = \frac{2}{3V_{sq}} Q_{f\_ref} \quad (40)$$

The reference current i_{qf_ref} stems from the control loop of DC bus voltage.

$$i_{qf\_ref} = C_{ADRC}(U_{dc\_ref} - U_{dc}) \quad (41)$$

C_{ADRC} : equation of ADRC controller.

From (34), (35) and (37), the following expression of DC bus voltage is deduced:

$$2U_{dc}\frac{dU_{dc}}{dt} = \frac{3V_{sq}}{C} i_{qf} - \frac{2U_{dc}}{C} i_{mr} \quad (42)$$

we set $W = U_{dc}^2$, we obtain:

$$\frac{dW}{dt} = -\frac{2\sqrt{W}}{C} i_{mr} + \frac{3V_{sq}}{C} i_{qf} \quad (43)$$

We put (43) in the canonical form of ADRC regulator:

$$\frac{dW}{dt} = f_w + b_0 u_w(t) \quad (44)$$

$$\text{where: } \begin{cases} f_w = -\frac{2\sqrt{W}}{C} i_{mr} + (\frac{3V_{sq}}{C} - b_0) i_{qf} \\ b_0 = \frac{3V_{sq}}{C} \; ; \; u_w = i_{qf} \end{cases}$$

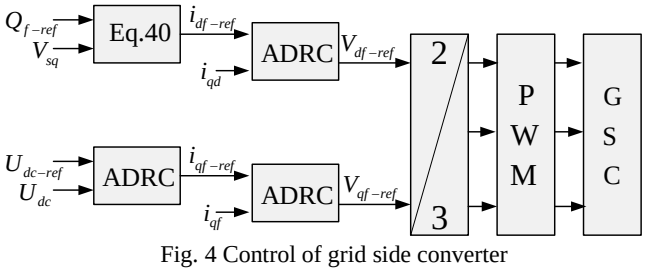

Fig. 4 Control of grid side converter

IV. Control Strategy of DFIG During Voltage Dip

The wind generators are very sensitive to grid disturbance and tend to disconnect during a voltage dip. In order to contribute to the stability of the grid, wind turbines must be controlled to stay connected even in the presence of a fault [2]-[13].

A. Control of stator flux during voltage dip

During the voltage dip, the stator flux decreases which causes demagnetization of the DFIG. At the end of the fault and when the grid voltage becomes normal, the generator can re-magnetize abruptly which leads to a high current call that could cause damages [3]-[4]. So, the stator flux control strategy must be used during voltage dip to keep the flux to a level ensuring the magnetization of the generator. This strategy is based on an ADRC closed loop control of both direct and quadrature components of the stator flux. The reference rotor currents are generated by these loops of flux control Φ_{sd} and Φ_{sq}.

$$i_{rd\_ref} = C_{ADRC}(\Phi_{sd\_ref} - \Phi_{sd}) \quad (45)$$

$$i_{rq\_ref} = C_{ADRC}(\Phi_{sq\_ref} - \Phi_{sq}) \quad (46)$$

During the voltage dip, the stator flux is not considered constant and aligned with the d-axis; therefore, its dynamics should not be neglected in the synthesis of controllers.

Substituting (11) and (12) into (6) and (8), the expressions of stator voltages become as follows:

$$V_{sd} = \frac{R_s}{L_s}\Phi_{sd} + \frac{d\Phi_{sd}}{dt} - R_s\frac{L_m}{L_s}i_{rd} - \omega_s\Phi_{sq} \quad (47)$$

$$V_{sq} = \frac{R_s}{L_s}\Phi_{sq} + \frac{d\Phi_{sq}}{dt} - R_s\frac{L_m}{L_s}i_{rq} + \omega_s\Phi_{sd} \quad (48)$$

To control the stator flux by ADRC regulator, we put (47) and (48) as follows:

$$\frac{d\Phi_{sd}}{dt} = f_{\psi d} + b_0 u_{\psi d}(t) \quad (49)$$

$$\text{where: } \begin{cases} f_{\psi d} = -\frac{R_s}{L_s}\Phi_{sd} + V_{sd} + \omega_s\Phi_{sq} + (\frac{R_s L_m}{L_s} - b_0)i_{rd} \\ b_0 = \frac{R_s L_m}{L_s}\ ;\ u_{\psi d} = i_{rd} \end{cases}$$

$$\frac{d\Phi_{sq}}{dt} = f_{\psi q} + b_0 u_{\psi q}(t) \quad (50)$$

$$\text{where: } \begin{cases} f_{\psi q} = -\frac{R_s}{L_s}\Phi_{sq} + V_{sq} + \omega_s\Phi_{sd} + (\frac{R_s L_m}{L_s} - b_0)i_{rq} \\ b_0 = \frac{R_s L_m}{L_s}\ ;\ u_{\psi q} = i_{rq} \end{cases}$$

The reference flux are chosen so that the stator flux is regulated around the forced flux.

$$\Phi_{sd\_ref} = \frac{V'}{\omega_s} \quad (51)$$

$$\Phi_{sq\_ref} = 0 \quad (52)$$

$V' = V_{sq}$ is the stator voltage during the fault.

Figure 5 shows the block diagram of DFIG control strategy during the voltage dip.

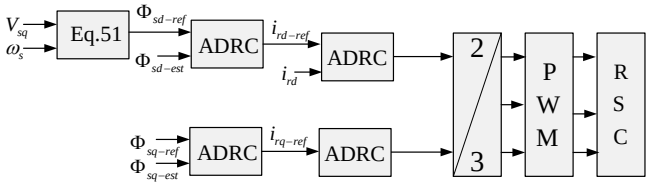

Fig. 5 Control of stator flux during voltage dip

B. Protection by crowbar

Maintaining the operation of the DFIG in a failure regime is limited by the relatively small dimensions of the rotor side converter. The latter lacks the capacity to withstand rotoric over-currents and over-voltages produced during the voltage dip. In this case, an additional physical protection of the system by resistive circuits called « crowbar » is deemed necessary (figure 6) [9]-[13]-[15]-[16].

The crowbar is a short-circuiting device of the rotor coiling in case of fault. Its main role is to limit the current in rotor and the voltage in DC bus. At the appearance of the voltage dip and when the crowbar is activated (Scrow=1), the rotor side converter is disconnected and the grid side converter stays connected to maintain the voltage DC bus constant. To ensure the controllability of the generator for the maximum of time during the voltage dip, the crowbar is activated during 0.01s only at the appearance and disappearance of the fault. The rotor side converter resumes its normal operation when the crowbar is disconnected from the rotor coiling [4]-[13].

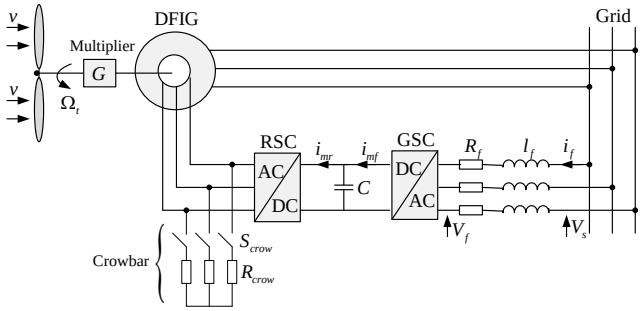

Fig. 6 Wind system with crowbar

V. Simulation Results

To study the influence of voltage dip on the control strategy proposed, a symmetrical three-phase of 60% and a duration of 500 ms voltage dip is applied to the DFIG (figure 7). Since the duration of voltage dip is smaller than the fluctuations in wind speed, we consider the wind speed constant during the fault and equals 10m/s. R_{crow} resistance of crowbar circuit is taken to be $40 * R_r$. The parameters of the simulated wind system in Matlab-Simulink environment as well as the parameters of regulators are given in the appendix.

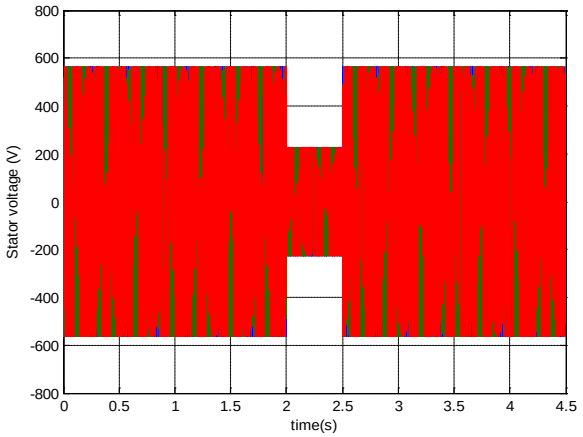

Fig. 7 Stator voltage

The rotor speed is shown in figure 8. It is found that, at the appearance of the voltage dip at t=2s, speed increases almost linearly during the period of the fault. This acceleration of the turbine is due to the inertial storage power. Indeed, during the voltage dip, the power transmitted to the grid decreases and that captured by the turbine is considered constant, which causes an excess of power within the system. This power excess is stored mechanically in the turbine and therefore causes its acceleration. At the disappearance of the fault and after a transient regime of 1.5s, the rotor speed returns to its value before the voltage dip (150 m/s) and the turbine returns to its normal operation.

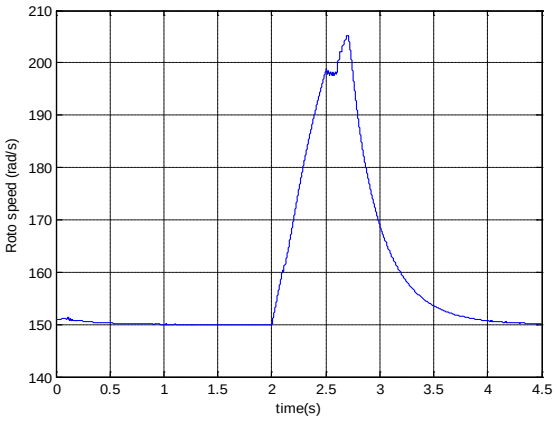

Fig. 8 Rotor speed

Figures 9 and 10 show the evolution of the electromagnetic torque of the generator. At the appearance of the fault, torque decreases and cancels after a transitional regime, which further explains once again the acceleration of the turbine. It resumed its value before the voltage dip 0.7s after the fault disappears, contributing to the slowing of the turbine.

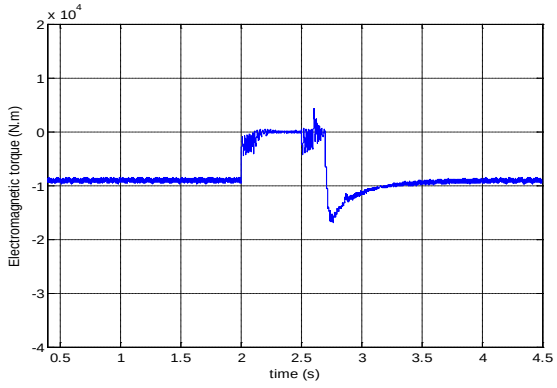

Fig. 9 Electromagnetic torque

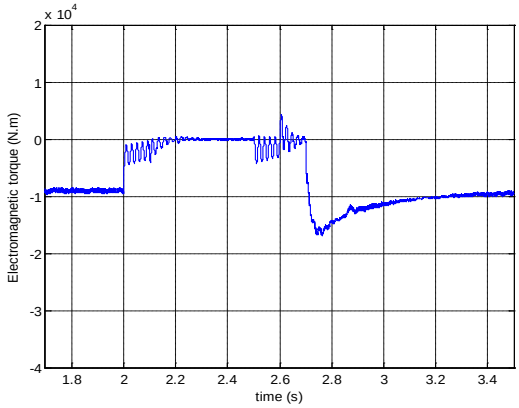

Fig. 10 Zoom on electromagnetic torque

Figure 11 shows the DC bus voltage during the voltage dip. Although, during the fault, this voltage increases due to the amount of an extra power fed into power converters, the control system can regulate this voltage to the reference value during the fault. After the disappearance of voltage dip, the DC bus voltage perfectly follows its reference exactly as before the fault occurred.

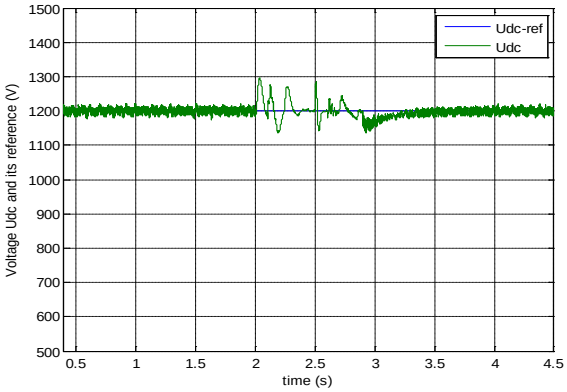

Fig. 11 Voltage Udc and its reference

Figure 12 shows the stator active power during voltage dip. At the appearance of the fault and after a transitional regime, active power becomes very low. The transfer of the stator active power of the generator to the grid resumes after the disappearance of the voltage dip and regains its initial value 0.7s after the resoration of the stator voltage.

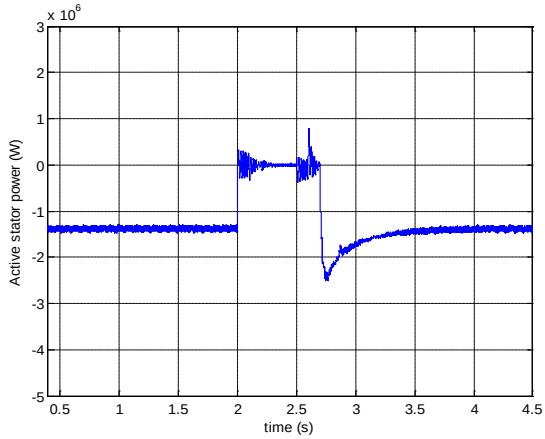

Fig. 12 Active stator power

Figures 13 and 14 show the stator reactive power during voltage dip. This power is not null during the fault, which shows that the control strategy of the stator flux allows the magnetization of the generator during the voltage dip. Reactive power perfectly regains its reference 0.4s after the return of the voltage supply.

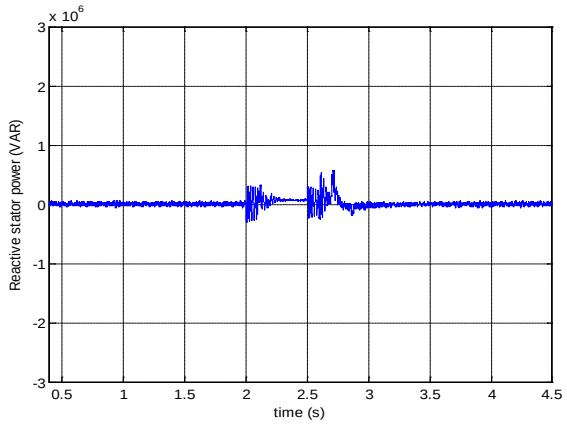

Fig. 13 Reactive stator power

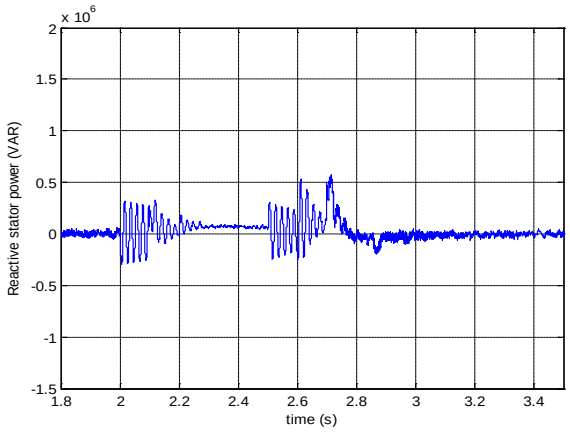

Fig. 14 Zoom on reactive stator power

Figure 15 shows the rotor current before, during and after the voltage dip. A current peak is observed at t=2.1s, instant of disconnection of crowbar after the appearance of the fault, and another peak is observed at t=2.6s, instant of disconnection of crowbar after the disappearance of voltage dip. The first peak current is due to the additional power introduced into the system following the decrease of the power transmitted to the grid during the voltage dip, while the second peak is the result of the re-magnetization of the generator. One second after the disappearance of the fault, the rotoric currents perfectly regain their forms and values before voltage-dip.

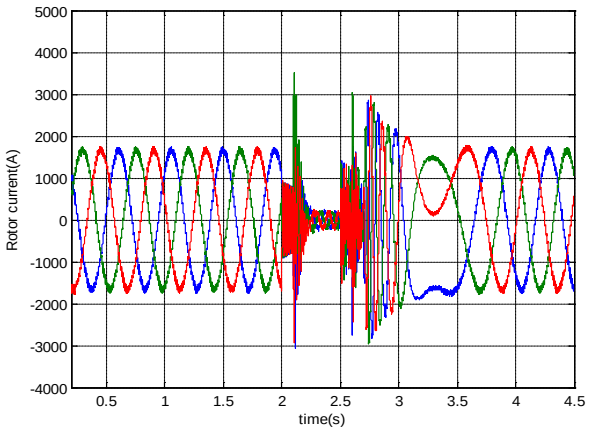

Fig. 15 Rotor current

Figures 16 and 17 show the evolution of direct and quadrature components of the rotor current. In a normal operation, the two components of the rotor current perfectly follow their references. During the voltage dip, the i_{rd} and i_{rq} currents regain their references after a transitional regime characterized by oscillations that appear at the beginning and the end of the fault.

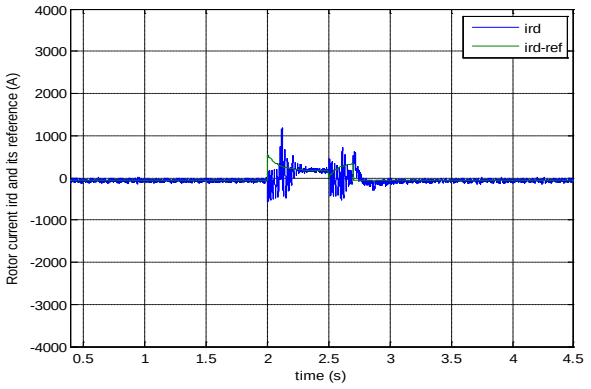

Fig. 16 Rotor current i_{rd} and its reference

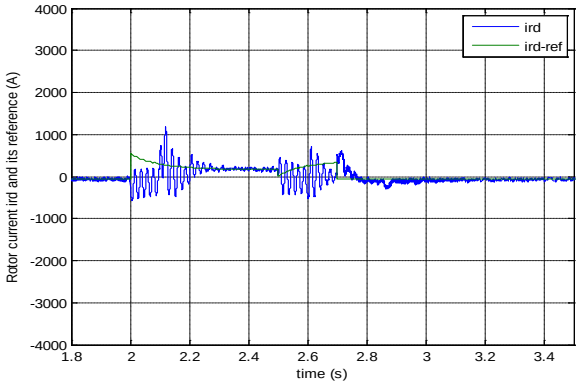

Fig. 17 Zoom on rotor current i_{rd} and its reference

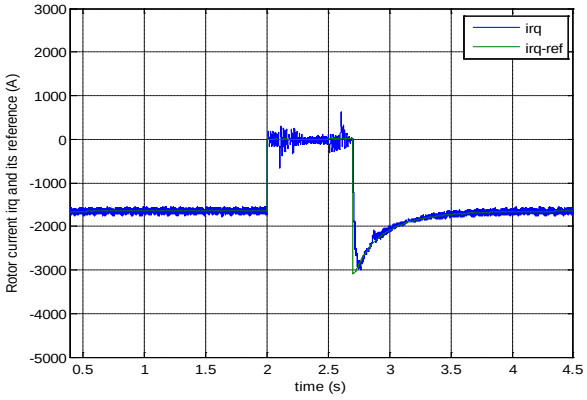

Fig. 18 Rotor current i_{rq} and its reference

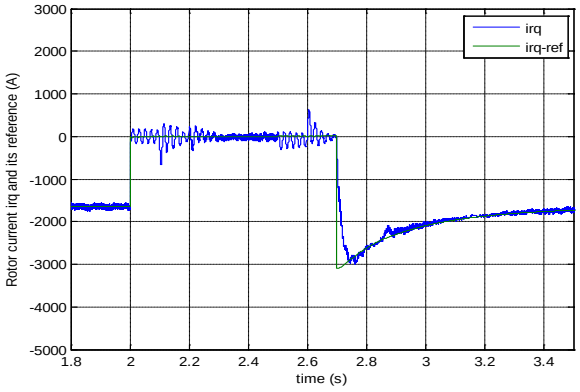

Fig. 19 Zoom on rotor current i_{rq} and its reference

Figures 20 and 21 show the direct and quadrature components of the stator flux. It is found that the flux during voltage dip is equal to the value of the forced flux after a transitional regime characterized by oscillations of the flux. After the fault, the two components of the stator flux perfectly follow their values before the voltage dip. The control of the stator flux is maintained after the fault for some time (0.01s in this simulation) for the generator to re-magnetize properly and returns to its normal operation.

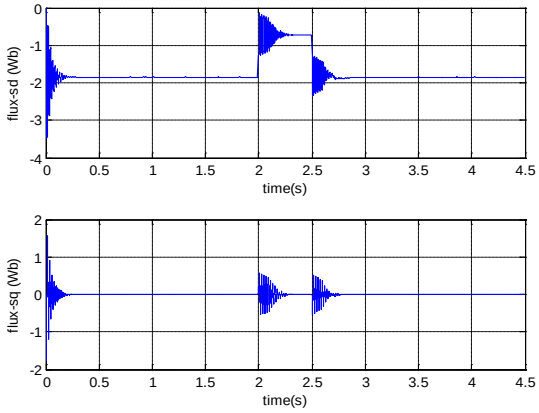

Fig. 20 Stator flux

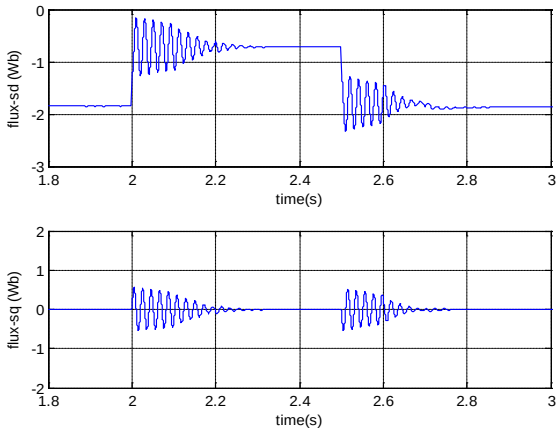

Fig. 21 Zoom on stator flux

VI. Conclusion

In this article, we have been interested in the behavior of internal greatness of the variable speed wind system during the voltage dip, and we have proposed a control strategy based on the ADRC control loops to improve the controllability of DFIG and maintaining its connection to the grid during and after a voltage dip.

The control strategy of the stator flux proposed in this study takes into account the stator flux dynamics and allows magnetization of the generator during the voltage dip and a few milliseconds after its disappearance. The rotor current and DC bus voltage are limited by the use of the crowbar that can evacuate a portion of power excess generated after the reduction of the power transmitted to the grid during the voltage dip.

Simulation results have been presented to show the validity and effectiveness of the stator flux control strategy based on an ADRC method, which has allowed the DFIG to staying connected during the voltage dip and regain its normal operation after a few hundred milliseconds once the fault disappears.

Appendix

Doubly fed induction generator parameters

Rated power 1.5 MW

Stator and rotor resistance: $R_s = 10.3m\Omega$, $R_r = 8.28m\Omega$

Stator and rotor inductance: $L_s = 27.2401mH, L_r = 27.0777mH$

Mutual inductance: $L_m = 26.96\ mH$

Number of pole pairs: $p = 2$

Resistance of crowbar $R_{crow} = 331.2\ m\Omega$

Turbine parameters

Radius of the turbine $R = 39m$

Gain multiplier $G = 65$

Inertia total moment $J = 60Kg.m^2$

Air density $\rho = 1.225Kg/m^2$

Coefficient of viscous friction $f = 0.1$

Optimal tip speed ration $\lambda_{opt} = 8.1$

Maximal power coefficient $C_{pmax} = 0.41$

Connecting to the grid parameters

Filter inductance $L_f = 2.5mH$

Filter resistance $R_f = 75m\Omega$

DC link capacity $C = 5000\mu F$

ADRC controller parameters

Rotor currents controller gain $K_{p\_r} = 100$

Rotor currents parameter $b_{r0} = 2532.2$

Observation parameters of the loop currents rotor $\beta_{1r} = 600$, $\beta_{2r} = 9e^4$

Filter currents controller gain $K_{p\_f} = 300$

Filter currents parameter $b_{f0} = -400$

Observation parameters of the loop currents filter $\beta_{1f} = 1800$,$\beta_{2f} = 81e^4$

DC link voltage controller gain $K_{p\_c} = 100$

DC link voltage parameter $b_{c0} = 3.3941e^5$

Observation parameters of the loop DC link voltage $\beta_{1c} = 600$, $\beta_{2c} = 9e^4$

Stator flux controller gain $K_{p\_\psi} = 1.5$

Stator flux parameter $b_{\psi 0} = 0.0102$

Observation parameters of the loop stator flux $\beta_{1\psi} = 9$, $\beta_{2\psi} = 20.25$

REFERENCES

[1] "Global wind statistics 2014", GWEC report, February 2015, [Online].Available:www.gwec.net/wpcontent/uploads/2015/02/GWEC_Globalwindstats2014_FINAL_10.2.2015.pdf

[2] J. Morren, S. W. H. de Haan, " Ridethrough of wind turbines with doubly fed induction generator during a voltage dip," IEEE Transactions on energy conversion, vol. 20, No. 2, pp. 435-441, June 2005.

[3] J. Lopez, P. sanchis, X. Roboam, L. Marroyo, "Dynamic behavior of the doubly fed induction generator during three-phase voltage dips," *IEEE Transactions on energy conversion*, vol. 22, No. 3, September 2007.

[4] L. Peng, ''Reconfiguration du dispositive de commande d'une éolienne en cas de creux de tension," Thèse de doctorat, No d'ordre 122, Ecole central de Lille, juin 2010.

[5] F. K. A. Lima, A. Luna, P. Rodriguez, E. H. Watanabe, F. Blaabjerg, "Rotor voltage dynamic in the doubly fed induction generator during grid faults," *IEEE Transactions on power electronics*, vol. 25, No. 1, January 2010.

[6] R. Chakib, A. Essadki, M. Cherkaoui, "Modeling and control of a wind system based on a DFIG by active disturbance rejection control," *International review on modelling and simulations (IREMOS)*, vol. 7, No. 4, pp. 626-637, August 2014.

[7] X. Zheng, D. Guo, "A novel ride-through control strategy of DFIG wind generator under grid voltage dip," *Journal of information and computational science*, vol. 8, N°. 3, pp. 579-591, 2011.

[8] J. Han, "From PID to active disturbance rejection control," *IEEE Transactions on industrial electronics*, vol. 56, No. 3, March 2009.

[9] C. Wessels, F. W. Fuchs, "Fault ride through of DFIG wind turbines during symmetrical voltage dip with crowbar or stator current feedback solution," *IEEE energy conversion congress and exposition (ECCE)*, 12-16 september 2010 Atlanta, pp. 2771-2777.

[10] F. Blaabjerg, M. Liserre, K. Ma, "Power electronics converters for wind turbine systems," *IEEE Transactions industry applications*, Vol. 48, no. 2, March/April 2012.

[11] F. Blaabjerg, Z. Chen, R. Teodorescu, F. Iov, "Power electronics in wind turbine Systems," *IEEE Power electronics and motion control conference IPEMC*, 14-16 august 2006 Shanghai, pp. 1-11, Doi: 10.1109/IPEMC.2006.4777946.

[12] K. Eftichios, K. Kostas, "Design of a maximum power tracking system for wind energy conversion applications," *IEEE Transactions on industrial electronics*, vol. 53, No. 2, pp. 486-494, April 2006.

[13] C. Wessels, F. Gebhardt, F. W. Fuchs, "Dynamic voltage restorer to allow LVRT for a DFIG wind turbine," *IEEE international symposium on industrial electronics (ISIE)*, 4-7 july 2010, pp. 803-808, Doi 10.11109/ISIE.2010.5637336.

[14] O. Zheng, " On active disturbance rejection control: stability analysis and applications in disturbance decoupling control", Ph.D dissertation, dept elect. Computer. Eng, Cleveland state university USA, july 2009.

[15] Z. peng, H. Yikang, "Control strategy of an active crowbar for DFIG based wind turbine under grid voltage dips," *IEEE international conference on electrical machines and systems (ICEMS)*, 8-11 october 2007 Seoul, pp. 259-264W.

[16] S. Chandrasekaran, C. Rossi, D. Casadei, A. Tani, "Improved control strategy for low voltage ride through capability of DFIG with grid code requirements," *Electrical & computer engineering: An international journal (ECIJ)*, vol. 2, No. 2, June 2013.

Rachid CHAKIB was born in Rabat, Morocco in 1973. He received the Engineer Degree in Electrical Engineering, from National Higher School of Electricity and Mecanics (ENSEM), Casablanca, Morocco, in 1997. He is currently preparing a PhD thesis in the department of Electrical Engineering of Mohammedia School of Engineer (EMI), university Mohamed V, Rabat, Morocco.

His research areas include renewable energy, machine control and electrical systems.

Mohamed CHERKAOUI was born in Marrakech, Morocco in 1954. He received the Engineer Degree in Electrical Engineering, from Mohammedia Engineering School (EMI), Rabat, Morocco, in 1979. He received his PhD degree from Institut National Polytechnique de Lorraine, Nancy, France in 1985. In 1986, he joined the university of Caddi Ayyad of Merrakech as a researcher professor. In 1995, he moves then to the Mohammedia Engineering School (EMI), Rabat, as a professor of higher education and head of Electrical engineering department.

Prof. CHERKAOUI is a director of the research laboratory in electrical power and control of the Mohammedia engineering school (EMI), Rabat,Morocco. He is also an expert with Moroccan ministry for higher education and with industrialists to matters related to the energetic efficiency.His main research interests are renewable energy and control of electrical systems.

Ahmed ESSADKI is currently a Professor and university research professor at the electrical engineering department of ENSEF, Mohamed V souissi university Morocco**.** In 2000, he received his PhD degree from Mohammedia Engineering School (EMI), Morocco. From 1990 to 1993, he pursued his master program at UQTR university, Quebec Canada, respectively, all in electrical engineering. His current research interests include renewable energy, motor drives and power system. Dr ESSADKI is a member of RGE Lab in research group Leader.